

Article

Towards Understanding Relationships between Tension Property and Twinning Boundaries in Magnesium Alloy

Jianhui Bai ^{1,*}, Pengfei Yang ², Zhiyuan Yang ³, Qi Sun ³ and Li Tan ^{4,*}

¹ School of Aviation and Mechanical Engineering, Changzhou Institute of Technology, Changzhou 213032, China

² Tribology Research Institute, School of Mechanical Engineering, Southwest Jiaotong University, Chengdu 610036, China; yangpengfei@my.swjtu.edu.cn

³ Key Laboratory of Advanced Technologies of Materials (Ministry of Education), School of Material Science and Engineering, Southwest Jiaotong University, Chengdu 610036, China; 2016114187@my.swjtu.edu.cn (Z.Y.); sunqi211282@swjtu.edu.cn (Q.S.)

⁴ School of Materials Science and Engineering, Chongqing University of Technology, Chongqing 400044, China

* Correspondence: baijh@cit.edu.cn (J.B.); tanli@cqut.edu.cn (L.T.); Tel.: +86-199-7510-8887 (J.B.); +86-139-8347-2537 (L.T.)

Abstract: Although pre-induced $\{10\bar{1}2\}$ twins could strengthen magnesium and its alloys, the origin of such a strengthening phenomenon remains questionable. This is because twins can simultaneously change the size of grains and the texture features of the initial material. In the present work, the effect of pre-induced $\{10\bar{1}2\}$ twins on the tension property of an extruded magnesium alloy has been investigated through a combination of electron backscatter diffraction, transmission electron microscope, and mechanical tests. Samples with and without $\{10\bar{1}2\}$ twinning boundaries, but possessing an almost identical texture characteristic, were prepared by pre-compression perpendicular to the extrusion direction. Subsequently, these pre-strained samples were tensioned along the extrusion direction. The results indicate that the pre-induced $\{10\bar{1}2\}$ twinning boundaries can indeed enhance the tension strength of magnesium alloys, but only slightly. The effect is closely associated with the amount of pre-strain. Correspondingly, the possible mechanisms behind such phenomena are given and discussed.

Keywords: twin; twinning boundary; texture; strength; magnesium alloy



Citation: Bai, J.; Yang, P.; Yang, Z.; Sun, Q.; Tan, L. Towards Understanding Relationships between Tension Property and Twinning Boundaries in Magnesium Alloy. *Metals* **2021**, *11*, 745. <https://doi.org/10.3390/met11050745>

Academic Editor: Hamid Jahed

Received: 2 April 2021
Accepted: 25 April 2021
Published: 30 April 2021

Publisher's Note: MDPI stays neutral with regard to jurisdictional claims in published maps and institutional affiliations.



Copyright: © 2021 by the authors. Licensee MDPI, Basel, Switzerland. This article is an open access article distributed under the terms and conditions of the Creative Commons Attribution (CC BY) license (<https://creativecommons.org/licenses/by/4.0/>).

1. Introduction

Magnesium and its alloys have obtained extensive attention for their application in the automotive and aerospace industries because of their outstanding properties, such as low density and high specific strength [1]. However, as a typical metal with a hexagonal close-packed (hcp) structure, in addition to dislocation slips, deformation twins also play an important role during plastic deformation, especially at low temperatures [2–4]. This leads to magnesium and its alloys possessing a strong, basal texture characteristic after rolling and extrusion processes, and exhibiting a remarkable tension/compression yield asymmetry, due to the polar feature of deformation twins [5–7]. Besides, magnesium and its alloys also exhibit a low yield strength at room temperature [1,4–8]. These characteristics significantly restrict their processing, design, and applications, especially as load-bearing components. A number of previous publications have indicated that refining grain size is an effective procedure to reduce the disadvantages of magnesium alloys, and, correspondingly, several attempts have been made to produce magnesium alloys by refining grain size [9–12]. For example, by means of equal-channel angular pressing (ECAP), Li et al. [9] successfully obtained AZ60 magnesium alloy with grain size of $\sim 0.8 \mu\text{m}$ after eight passes and improved the mechanical property of magnesium alloy at a high strain rate.

Recently, some publications have suggested that pre-induced $\{10\bar{1}2\}$ twins can also refine the grain size of initial magnesium alloys, resulting in the enhancement of their yield

strength [13–16]. The authors suggested that $\{10\bar{1}2\}$ twinning boundaries (TBs) may have a similar function to traditional high-angle grain boundaries that can strongly impede the movement of matrix dislocations [15–17]. As a consequence, matrix dislocations have to halt and be piled up in the front of $\{10\bar{1}2\}$ TBs during plastic deformation, leading to the strengthening effect in magnesium alloys. By contrast, based on experimental observations, M.R. Barnett suggested that, compared to grain refined by TBs, reorientation of the c-axes by twins might play a more important role in the strengthening effect in magnesium alloys [18]. Knezevic et al. [19] further pointed out that the main contribution of $\{10\bar{1}2\}$ twins to hardening came from texture hardening, namely that the initial grains with soft orientations were changed into new grains with hard orientations by $\{10\bar{1}2\}$ twins. Similar conclusions were also reported by Wang et al. [20]. More recently, a series of works conducted by Chen et al. [21,22] even suggested that, during plastic deformation, $\{10\bar{1}2\}$ TBs appeared to be an ineffective barrier for the matrix dislocation movement, indicating that the strength caused by $\{10\bar{1}2\}$ TBs might be negligible. From those above studies, it is quite clear that pre-induced $\{10\bar{1}2\}$ twins can significantly influence the mechanical property of magnesium alloys, although a consensus has not been reached about the causes of these effects.

For this purpose, in the present work, the influence of pre-induced $\{10\bar{1}2\}$ twinning boundaries on the strength of extruded AZ31 samples was investigated by a combination of electron backscatter diffraction (EBSD), transmission electron microscope (TEM) and mechanical tests. The results show that $\{10\bar{1}2\}$ TBs themselves can indeed enhance the strength of magnesium alloy, but only slightly. Accordingly, the possible mechanisms behind such interesting phenomena are discussed. These findings are expected to provide a new insight into the role of the $\{10\bar{1}2\}$ twin in magnesium and other metals with hcp structure.

2. Experiments

2.1. Initial Material and Deformation

It should be noted that for magnesium and its alloys, when $\{10\bar{1}2\}$ TBs are introduced, the texture feature is usually changed. Thus, one intractable problem is how we can fabricate a magnesium alloy sample that contains $\{10\bar{1}2\}$ TBs but still possesses the initial texture feature. In this case, the influence stemming from pre-induced TBs themselves can be evaluated conveniently. It is well known that extruded magnesium alloys usually possess a strong basal fiber texture, namely that the (0001) crystallographic direction of grains is largely perpendicular to the extrusion direction (ED), and randomly distributed around the ED [8]. On the other hand, as indicated in references [23,24], the $\{10\bar{1}2\}$ twin prefers to rotate the lattices of initial grains into the external load direction. Accordingly, based on the features of extruded magnesium alloy and the $\{10\bar{1}2\}$ twin, we may fabricate a special sample which satisfies the above requirements.

The material used in the current work was an extruded AZ31 (3 wt% Al–1 wt% Zn) magnesium alloy rod. As presented in Figure 1a, the as-received material displays a twin-free microstructure feature with an average grain size of $\sim 30 \mu\text{m}$. The corresponding pole figures shown in Figure 1b indicate that the extruded rod presents a typical extrusion texture with (0001) poles largely perpendicular to the ED and randomly distributed around the ED. In order to obtain samples with pre-induced $\{10\bar{1}2\}$ TBs, some rectangular parallelepiped samples with the dimensions of $100 \text{ mm} \times 5 \text{ mm} \times 10 \text{ mm}$ (ED \times ERD \times ETD) were first cut from the center of the as-received material by electrical discharge machining (EDM), where the ERD and ETD are referred to as the radial direction and tangential direction of the extrusion rod, respectively. Then, one part of these samples was subjected to pre-compression along ERD at a strain rate of $1 \times 10^{-3} \text{ s}^{-1}$ to a strain of $\sim 0.9\%$ and $\sim 1.3\%$. Subsequently, all of these samples, including samples with and without pre-compression, were annealed at $200 \text{ }^\circ\text{C}$ for 6 h to remove the dislocations caused by pre-strain, while maintaining the twin structure [14]. Accordingly, those samples with and without pre-

strain subjected to anneal are denoted as ERD0.9CA, ERD1.3CA and ERD0CA, respectively, in the succeeding paragraphs.

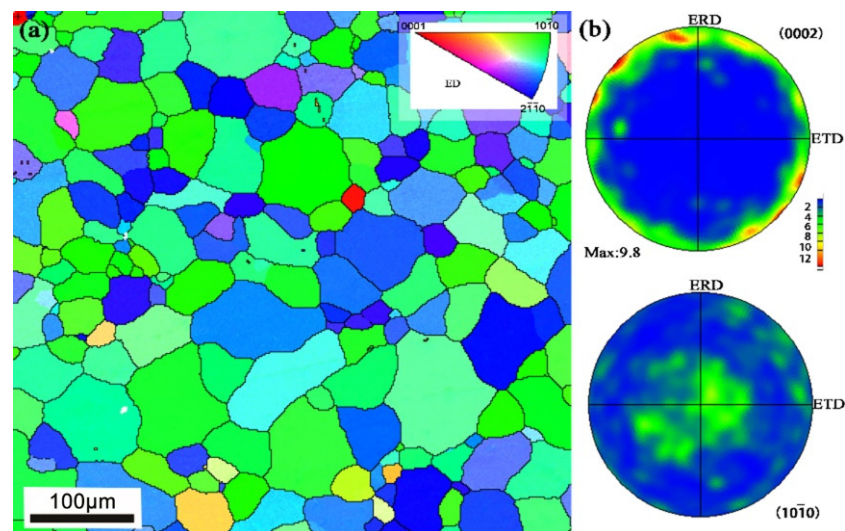


Figure 1. (a) EBSD map using inverse pole figure (IPF) coloring shows the initial microstructure of as-received AZ31 magnesium alloy rod. (b) The corresponding pole figure of as-received AZ31 magnesium alloy rod.

In order to investigate the effect of pre-induced $\{10\bar{1}2\}$ TBs on the subsequent tension property, five dog-bone shaped tension samples with dimensions of the rectangular gage section of $50 \text{ mm} \times 4 \text{ mm} \times 5 \text{ mm}$ (ED \times ERD \times ETD) were cut from ERD0.9CA, ERD1.3CA and ERD0CA by EDM technology, respectively. Then, tension mechanical tests along ED were performed at a strain rate of $1 \times 10^{-3} \text{ s}^{-1}$. In order to measure the accurate strain, an extensometer (E98918, Epsilon) was mounted on every sample. Three samples for each condition were stretched to a cracking point for a better understanding of the relationship between microstructure feature and macroscopy performance. Two tension tests for each condition were disrupted at a strain of $\sim 1.2\%$. Correspondingly, these samples are marked as ERD0.9CA-ED1.2T, ERD1.3CA-ED1.2T and ERD0CA-ED1.2T, respectively.

2.2. EBSD and TEM Examinations

The microstructural characteristics of the ERD-ETD cross section of these deformed samples were examined by EBSD. Before EBSD examination, the investigated surfaces were ground mechanically with green SiC papers from 500# to 4000#, followed by electropolishing (voltage: 15 V, electric current: 0.15 A, temperature: -30° , dwell time: 150 s) using the commercial AC2 solution. The EBSD investigations were performed via the HKL Channel 5 system equipped in FEI Nova 400 FEG-SEM. The step size used in the current EBSD examinations was $1 \mu\text{m}$. For TEM and high-resolution TEM (HRTEM) observations, the samples were cut for the center of ERD1.3CA, and then thinned by grinding to $50 \mu\text{m}$, followed by the low-temperature ion thinning technique. Subsequently, TEM and HRTEM were performed by a FEI Tecnai F20-G² electron microscope with a voltage of 200 kV.

3. Results

3.1. Mechanical Properties

Stress–strain curves under tension along ED for the ERD0.9CA, ERD1.3CA and ERD0CA are given in Figure 2. It can clearly be seen that, for all the samples, the flow stresses present a typical dislocation slip dominated deformation feature, irrespective of the amount of pre-strain [25]. This suggests that almost no twinning or detwinning process takes place during the tension process [23,24]. Meanwhile, the mechanical properties of all three samples derived from the curves are listed in Table 1. Evidently, the yield stress

of 0% pre-strained samples (ERD0CA) is the lowest, only about 178 MPa. As pre-strain increases, the yield stress also increases to 182 MPa and 186 MPa for ERD0.9CA and ERD1.3CA, respectively, which are only slightly higher than that of the samples without pre-strain. Interestingly, with increasing strain, the difference between the tension stresses of these three kinds of samples also increases. As indicated in Table 1, when the strain reaches 3%, the stress for ERD1.3CA is higher than that for ERD0CA, but not by much (~15 MPa). In addition, the elongations of these three kinds of sample are presented in Table 1. The elongation of ERD0CA is ~21%, decreasing to ~19% and ~17% for ERD0.9A and ERD1.3A, respectively.

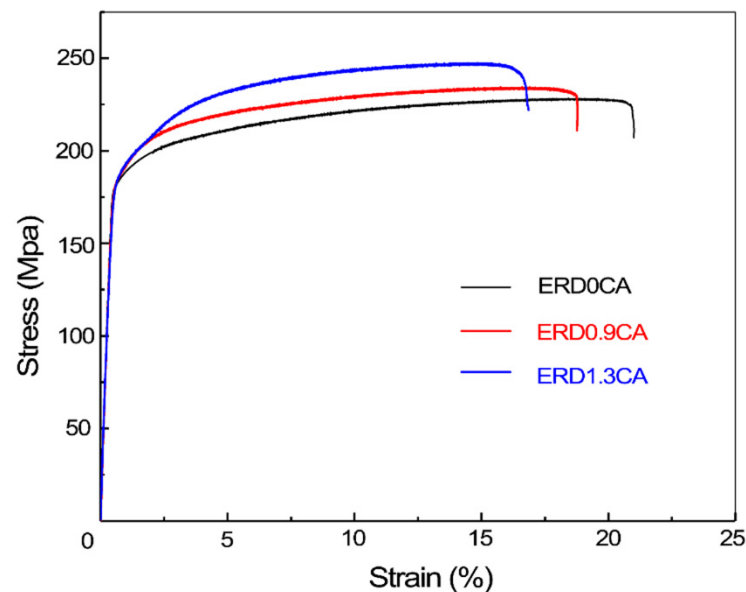


Figure 2. Typical stress–strain curves of pre-strained samples under tension along extrusion direction (ED) of magnesium alloy rod.

Table 1. Yield stress (0.2% proof stress) and stresses corresponding to different strains and elongation of the samples with and without pre-strain during tension along extrusion direction. Before tension, all these samples are annealed. The pre-strains for the three kinds of samples are 0 (ERD0CA), 0.9% (ERD.09CA) and 1.3% (ERD0CA), respectively.

	Yield Stress (MPa)	Stresses Corresponding to Different Strains (MPa)				Elongation (%)
		1%	3%	5%	10%	
ERD0CA	178	184	205	211	221	21
ERD0.9CA	182	192	213	221	229	19
ERD1.3CA	186	193	220	232	244	17

3.2. Microstructure Features Caused by Pre-Strain

It is well known that $\{10\bar{1}2\}$ extension twins are readily formed in magnesium alloys when the external compression load is perpendicular to the c-axes of the grains. According to the pole figures shown in Figure 1b, the (0001) poles of the initial material used in the present work are largely perpendicular to the ED and randomly distributed around the ED. Thus, when pre-compression along ERD takes place, twins may be formed theoretically in the grains, whose c-axes largely deviate from ERD. The EBSD maps shown in Figure 3a–c exhibits a typical microstructure feature of ERD1.3CA. Apparently, a number of $\{10\bar{1}2\}$ twins, whose boundaries are colored in red, are indeed produced in such samples. In the current EBSD analysis, the tolerance within $\pm 5^\circ$ of theoretical misorientation and axis ($86^\circ < 11\bar{2}0 >$) was acceptable. The other grain boundaries with misorientation angle values $> 10^\circ$ are denoted in black. Figure 3b–d displays the EBSD maps using an

inverse pole figure (IPF) coloring, which show the same areas as presented in Figure 3a–c, respectively. Obviously, within some grains (such as grains 2 and 5), no twins occur. This is because the c-axes of these grains are nearly parallel to the ERD, as indicated by the inserted crystalline structure cells, which is unfavorable for the formation of twins [14,15]. Meanwhile, the corresponding (0001) pole figures of Figure 3b–d are also inserted. More interestingly and importantly, it can be seen that the (0001) pole figures of these pre-strained samples are strongly perpendicular to the ED and randomly distributed around the ED, almost identical to that of the initial material (see Figure 1b).

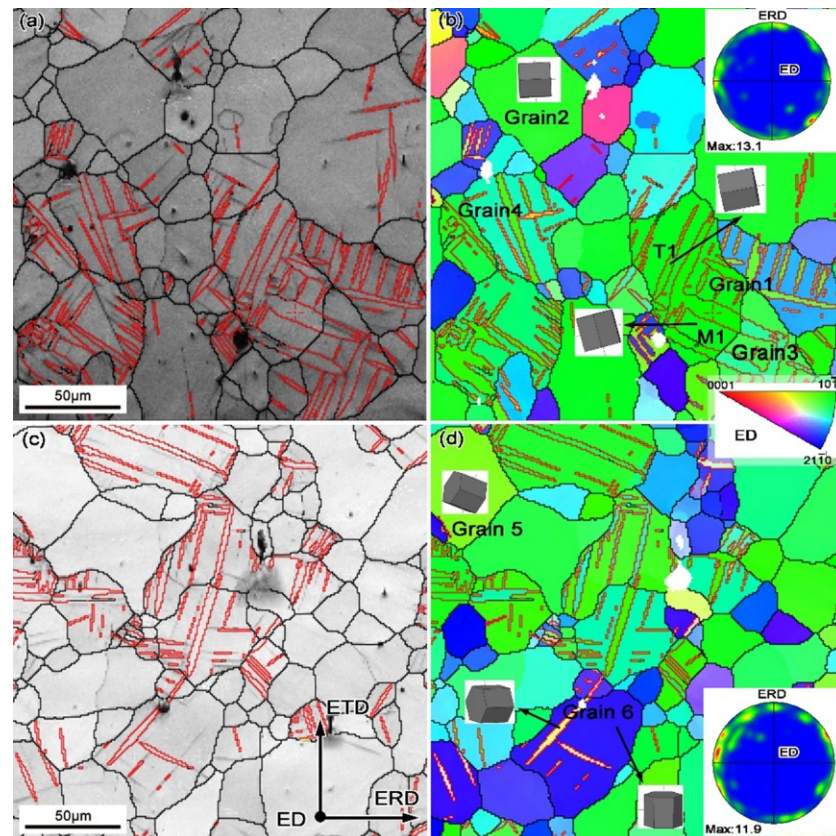


Figure 3. Typical EBSD results of 1.3% pre-strained and annealed samples (ERD1.3CA) in band contrast (a,c) and inverse pole figure maps (b,d). Boundaries of $\{10\bar{1}2\}$ twins are colored in red. The corresponding (0001) pole figures are inserted.

For a better understanding of the texture feature of these pre-strained samples, two grains containing twinned regions (grain 1 and grain 4) in Figure 3 are selected to perform texture examination, as presented in Figure 4. The IPF coloring EBSD maps of grain 1 and grain 2 are shown in Figure 4a,b, and the corresponding (0001) pole figures are exhibited in Figure 4c,d, respectively. In these images, the matrix regions and twinned areas are denoted as M_i ($i = 1, 3, 4$) and T_j ($j = 1, 2, 3, 4, 5$), respectively. When combining Figure 4a–c, the green circle representing the crystallographic orientation of M_1 is located at the edge of the (0001) pole figure, indicating the c-axis of M_1 is almost perpendicular to ED. Interestingly, after twinning, the crystallographic orientation of T_1 (denoted as the blue star) still lies at the edge of the (0001) pole figure (see Figure 4c). Additionally, similar changes to crystallographic orientation can be found in M_1 and T_2 , M_3 and T_3 , and M_4 and T_4 . These results unambiguously suggest that the textures before and after pre-compression along ERD are almost unchanged, which also agrees with the texture feature shown in Figure 3 and the observations in reference [26]. On the other hand, it should also be mentioned that, after pre-strain, some twinned regions, whose c-axes are not perpendicular to ED any longer, also exist in the pre-compression samples, just like T_5 in Figure 4b (indicated by

the orange star in Figure 4d). Such twinned areas influence the texture feature to some extent and may further affect the macroscopic performance of materials. However, the statistical results (not shown here) from about 800 grains reveal that such twinned areas are infrequent; only about 86 grains contain such twinned regions, resulting in the textures not changing much before or after pre-compression. This further indicates that the changes in mechanical properties caused by the texture associated with such twinned regions may be insignificant.

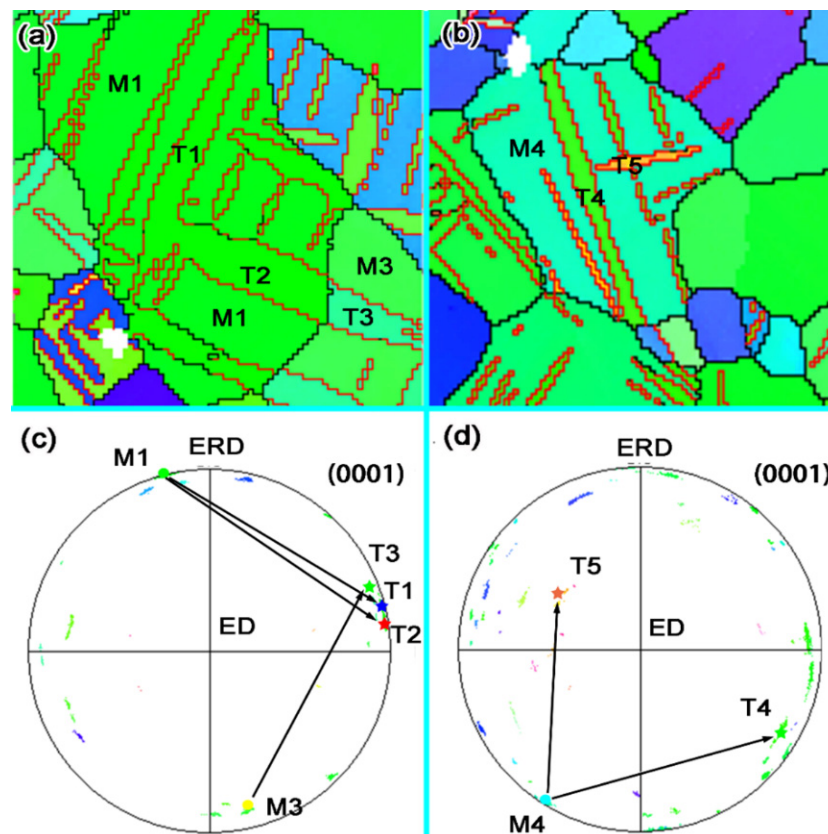


Figure 4. (a,b) Typical inverse pole figure EBSD maps showing the macrostructure feature of grain 1 and grain 4 in Figure 3. (c,d) The corresponding pole figures of regions shown in Figure 4c,d respectively.

3.3. Microstructures Investigated by TEM

The bright field TEM images in Figure 5a exhibit the microstructure features of sample ERD1.3CA. The electron beam is nearly along the $[11\bar{2}0]$ zone axis. In this case, the boundaries of $\{10\bar{1}2\}$ twins are almost parallel to the electron beam, i.e., edge-on. In Figure 5a, one deformation twin can be found, which should be formed during the pre-compression process. The selected-area electron diffraction (SAED) pattern taken from the region containing the twin and matrix is inserted, indicating that the twin observed here belongs to the $\{10\bar{1}2\}$ twinning mode. This is also consistent with the observations in Figure 3. Moreover, as can be seen in Figure 5a, both the twin and matrix in ERD1.3CA seem to be very clean, indicating that the density of dislocations should be low, which is ascribed to the annealing process. The HRTEM image shown in Figure 5b presents a typical interfacial feature of $\{10\bar{1}2\}$ twin in ERD1.3CA. The (0001) basal planes in twin and matrix are denoted by the white lines. The $\{10\bar{1}2\}$ TB consist of coherent boundaries and basal–prismatic interfaces, as marked by the red and yellow lines, respectively.

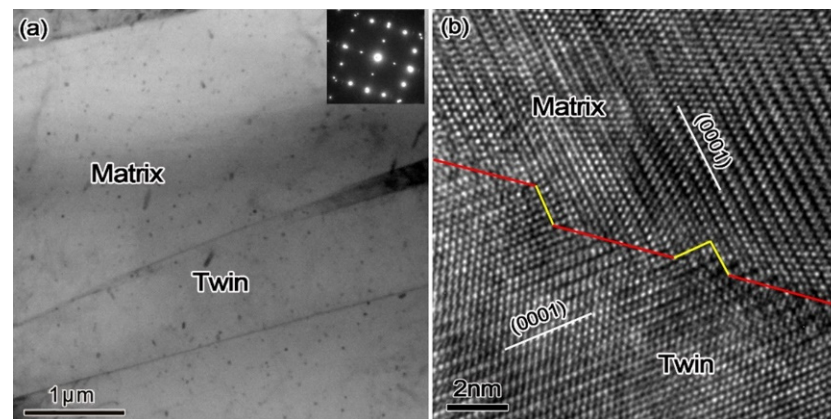


Figure 5. (a) Bright field TEM image showing the microstructure feature of 1.3% pre-strained and annealed samples (ERD1.3CA). The electron beam is nearly parallel to the $[11\bar{2}0]$ zone axis. (b) HRTEM image showing the interfacial structure of $\{10\bar{1}2\}$ twin in sample ERD1.3AC. The (0001) basal planes are denoted by the white lines. The $\{10\bar{1}2\}$ TB consist of coherent boundaries and basal-prismatic interfaces, as marked by the red and yellow lines, respectively.

4. Discussions

4.1. The Influence of Pre-Strain on the Tension Property

The influence of pre-induced $\{10\bar{1}2\}$ twins on the mechanical properties of magnesium alloys has been investigated extensively [14–17,24–27]. As shown in Figure 2 and Table 1, the yield stress (0.2% proof stress) of ERD1.3CA was the highest, about 186 MPa, while it was only slightly higher (~ 8 MPa) than that of ERD0CA (~ 178 MPa). This seems to indicate that the boundaries of pre-induced $\{10\bar{1}2\}$ twins play an insignificant role in the strengthening of magnesium alloy. However, on the other hand, it is worth noting that only about half of the grains could be twinned during pre-deformation in the current work, since the $\{10\bar{1}2\}$ twins prefer to be formed within the grains with the c-axes away from the external load direction about $45^\circ \sim 90^\circ$ (acute angle) [8]. If these TBs can strengthen the grains, the yield stress of those grains with twins will be enhanced. With this in mind, when the grains without twins enter the stage of plastic strain, the grains with twins may be still at the stage of elastic deformation. Consequently, the yield stresses of pre-strained samples shown in Figure 2 may mainly be attributed to the plastic deformation of those grains without twins.

In order to understand the contribution of pre-induced $\{10\bar{1}2\}$ TBs to the strength better, the stress values corresponding to larger strains were also extracted from the stress-strain curves, as shown in Table 1. It is conceivable that, with continued loading, those grains containing twins should also be involved in the deformation and accommodate the strain. Thus, the stress corresponding to a larger strain after yielding may reflect the influence of these pre-induced $\{10\bar{1}2\}$ TBs themselves on the tension property. As can be seen in Figure 2 and Table 1, the distinction between the strength of samples with and without pre-induced TBs gradually increases with increasing strain, suggesting that the pre-induced $\{10\bar{1}2\}$ TBs can affect the hardening behavior of magnesium alloy to some extent. Meanwhile, it is worth noting that, at the same strain, the stress of ERD1.3CA is always higher than that of ERD0.9CA and ERD0CA, indicating that the strengthening effect is also closely related to the level of pre-strain, which determines the amount of pre-induced $\{10\bar{1}2\}$ TBs. When the strain is about 3%, the tension stresses of ERD1.3CA (~ 219 MPa) are obviously higher than those of ERD0CA (~ 204 MPa) and ERD0.9CA (~ 213 MPa). It is assumed that when the strain reaches about 3%, the plastic deformation has already taken place within all of the grains. Thus, it may be concluded that the $\{10\bar{1}2\}$ TBs themselves can indeed enhance the strength of magnesium alloy, but limitedly, and the strengthening effect is related to the amount of pre-strain.

4.2. Strengthening Related to Twinning Boundaries

It is well known that the yield stress can be enhanced by introducing common high-angle grain boundaries (HAGBs) into the metals, according to an empirical equation, i.e., Hall–Petch relationship [28]

$$\sigma_y = \sigma_0 + kd^{-1/2} \quad (1)$$

where σ_y is the experimental yield stress of material, σ_0 is the friction stress when dislocation glides on the slip plane, d is the effective grain size and k is a constant related to the material itself. Inspired by this, $\{10\bar{1}2\}$ TBs are introduced in magnesium alloys as new grain boundaries in some publications to reduce the effective grain size and the mean free path of dislocations, leading to the enhancement of yield strength [14–17]. Our present work shows that pre-induced $\{10\bar{1}2\}$ TBs can indeed enhance the strength of magnesium alloys, especially their peak stress. It is assumed that every introduced TB can be considered as an “HAGB” in the present work; the average grain size of the twinned grains is estimated to be about $\sim 5 \mu\text{m}$. In reference [8], Y.C. Xin et al. proposed that, in the case of tension along ED of AZ31 rod, σ_0 varied around 123 MPa and the value of Hall–Petch slope (k) was about $245 \text{ MPa} \cdot \mu\text{m}^{-1/2}$. Thus, the corresponding stress which yields these grains can reach as high as $\sim 240 \text{ MPa}$, which is much higher than that caused by the pre-induced $\{10\bar{1}2\}$ TBs (see Table 1). This seems to indicate that, compared to HAGBs, the blocking effect of $\{10\bar{1}2\}$ TBs for the matrix dislocations is much weaker. Yu et al. [29] suggested that the weaker blocking effect of $\{10\bar{1}2\}$ TBs mainly originated from the much higher misorientation of $\{10\bar{1}2\}$ TBs (about 86°) than HAGBs. In addition to misorientation, the interfacial features of twins and grains are also remarkably different. In general, the atoms located at traditional HAGBs are usually chaotic [30], but the boundaries of $\{10\bar{1}2\}$ twins consist of coherent boundaries and basal–prismatic interfaces, and the atoms on these boundaries are usually regular and orderly, as shown in Figure 5b. Such interfacial characteristics of $\{10\bar{1}2\}$ twins were also observed in [22,31]. Presumably, the interfacial atom arrangements should also be responsible for the blocking effect. When the mobile matrix dislocations encounter general HAGBs, they will be strongly hindered and have to halt due to the distorted interfacial atom arrangement. In contrast, when the mobile matrix dislocations meet $\{10\bar{1}2\}$ TBs, the process of absorption or transformation would take place, rather than strong blocking and that, when the matrix dislocations interacted with $\{10\bar{1}2\}$ TBs, almost all of these matrix dislocations were absorbed or transmuted by TBs, rather than piled up in the front of TBs.

It should also be noted that, for the samples with pre-induced $\{10\bar{1}2\}$ twins, if detwinning takes place during the following tension process, the corresponding strength would be reduced due to the low activation stress required by detwinning [13]. Based on their experimental observations, Li et al. [26] found that the yield stresses of the samples with and without pre-induced $\{10\bar{1}2\}$ twins were almost equivalent and ascribed such a phenomenon to the detwinning process. In the current work, detwinning may play an insignificant role in reducing the strength caused by the pre-induced $\{10\bar{1}2\}$ twins. This is because the c -axes of twinned areas are nearly perpendicular to ED in the pre-strained samples (see Figures 3 and 4), which is unfavorable for the activation of detwinning during the subsequent tension along ED [14,24]. As presented in Figure 2, no yield plateau, which is a typical feature of $\{10\bar{1}2\}$ twinning or $\{10\bar{1}2\}$ detwinning, can be found indicating that almost no detwinning process takes place during the tension along ED for ERD0.9CA and ERD1.3CA. Moreover, the microstructural features of ERD1.3CA-ED1.2T are also presented in Figure 6. Abundant $\{10\bar{1}2\}$ twins can be identified here whose boundaries are colored in red. More importantly, almost no detwinning traces (as observed in reference [26]) can be found in the band contrast map shown in Figure 5a, further indicating that the detwinning process in ERD1.3CA-ED1.2T is not dramatic.

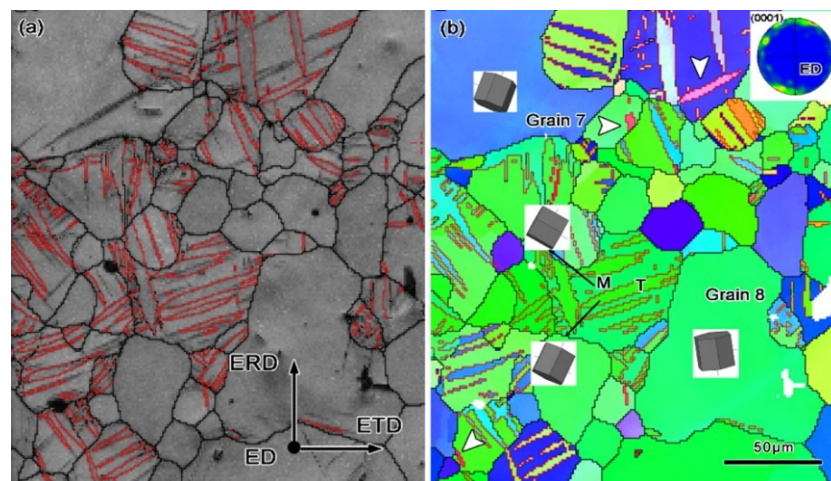


Figure 6. Typical EBSD results of the 1.3% pre-strained and annealed samples under tension along ED to a strain $\sim 1.2\%$ (ERD1.3CA-ED1.2T) in band contrast (a) and in inverse pole figure map (b). The boundaries of $\{10\bar{1}2\}$ twins are colored in red. The corresponding pole figure of the areas shown in Figure 5b is inserted at the right upper corner.

5. Conclusions

To conclude, the contribution of pre-induced $\{10\bar{1}2\}$ TBs to the tension property of magnesium alloy has been investigated using a combination of EBSD technology and mechanical tests. A comparative study about the strength of samples with and without pre-induced $\{10\bar{1}2\}$ twinning boundaries, but possessing an almost identical texture feature, was carried out. The experimental results show that the pre-induced $\{10\bar{1}2\}$ TBs can indeed improve the tension property of magnesium alloy, especially its peak stress, but limitedly. The weak strengthening effect of $\{10\bar{1}2\}$ twinning boundaries is thought to be closely related to their interfacial structure characteristics. Compared to general high-angle grain boundaries, the atoms located on the twinning boundaries are more orderly. These findings are expected to provide a new understanding of the twinning behaviors of magnesium and may help to design and develop magnesium alloys with superior properties.

Author Contributions: Q.S., L.T. and J.B. designed the experimental program; P.Y. and Z.Y. conducted the experiments; P.Y. analyzed the experimental results; J.B., P.Y. and Q.S. wrote the paper. All authors have read and agreed to the published version of the manuscript.

Funding: This work was co-supported by the National Natural Science Foundation of China (Nos. 51801165, 51901030), the Sichuan Science and Technology Program (No. 2020YFH0088), the Natural Science Foundation of the Jiangsu Higher Education Institutions of China (No. 20KJB430002), Natural Science Foundation of Chongqing (No. cstc2020jcyj-msxmX0877), and the Science and Technology Research Program of Chongqing Municipal Education Commission (No. KJQN201901118).

Informed Consent Statement: Not applicable.

Acknowledgments: The authors appreciate the valuable discussions with B. Song, School of Materials and Energy, Southwest University.

Conflicts of Interest: The authors declare no conflict of interest.

References

1. Mordike, B.L.; Ebert, T. Magnesium: Properties-applications-potential. *Mater. Sci. Eng. A Struct. Mater. Prop. Microstruct. Process.* **2001**, *302*, 37–45. [[CrossRef](#)]
2. Zhang, K.; Shao, Z.; Daniel, C.S.; Turski, M.; Pruncu, C.; Lang, L.; Robson, J.; Jiang, J. A comparative study of plastic deformation mechanisms in room-temperature and cryogenically deformed magnesium alloy AZ31. *Mater. Sci. Eng. A* **2021**, *807*, 140821. [[CrossRef](#)]
3. Zhang, K.; Zheng, J.-H.; Huang, Y.; Pruncu, C.; Jiang, J. Evolution of twinning and shear bands in magnesium alloys during rolling at room and cryogenic temperature. *Mater. Des.* **2020**, *193*, 108793. [[CrossRef](#)]

4. Christian, J.W.; Mahajan, S. Deformation twinning. *Prog. Mater. Sci.* **1995**, *39*, 1–157. [[CrossRef](#)]
5. Zeng, Z.R.; Zhu, Y.M.; Xu, S.W.; Bian, M.Z.; Davies, C.H.J.; Birbilis, N.; Nie, J.F. Texture evolution during static recrystallization of cold-rolled magnesium alloys. *Acta Mater.* **2016**, *105*, 479–494. [[CrossRef](#)]
6. Park, S.H.; Hong, S.-G.; Lee, J.H.; Huh, Y.-H. Texture evolution of rolled Mg-3Al-1Zn alloy undergoing a {10–12} twinning dominant strain path change. *J. Alloy. Compd.* **2015**, *646*, 573–579. [[CrossRef](#)]
7. Sun, Q.; Fang, X.Y.; Wang, Y.C.; Tan, L.; Zhang, X.Y. Changes in misorientations of twin boundaries in deformed magnesium alloy. *J. Mater. Sci.* **2018**, *53*, 7834–7844. [[CrossRef](#)]
8. Yu, H.H.; Li, C.Z.; Xin, Y.C.; Chapuis, A.; Huang, X.X.; Liu, Q. The mechanism for the high dependence of the Hall-Petch slope for twinning/slip on texture in Mg alloys. *Acta Mater.* **2017**, *128*, 313–326. [[CrossRef](#)]
9. Ghaderi, A.; Barnett, M.R. Sensitivity of deformation twinning to grain size in titanium and magnesium. *Acta Mater.* **2011**, *59*, 7824–7839. [[CrossRef](#)]
10. Choi, S.H.; Kim, J.K.; Kim, B.J.; Park, Y.B. The effect of grain size distribution on the shape of flow stress curves of Mg-3Al-1Zn under uniaxial compression. *Mater. Sci. Eng. A Struct. Mater. Prop. Microstruct. Process.* **2008**, *488*, 458–467. [[CrossRef](#)]
11. Li, B.; Joshi, S.; Azevedo, K.; Ma, E.; Ramesh, K.T.; Figueiredo, R.B.; Langdon, T.G. Dynamic testing at high strain rates of an ultrafine-grained magnesium alloy processed by ECAP. *Mater. Sci. Eng. A Struct. Mater. Prop. Microstruct. Process.* **2009**, *517*, 24–29. [[CrossRef](#)]
12. Zheng, R.X.; Bhattacharjee, T.; Shibata, A.; Sasaki, T.; Hono, K.; Joshi, M.; Tsuji, N. Simultaneously enhanced strength and ductility of Mg-Zn-Zr-Ca alloy with fully recrystallized ultrafine grained structures. *Scr. Mater.* **2017**, *131*, 1–5. [[CrossRef](#)]
13. Guo, X.; Ma, C.; Zhao, L.; Chapuis, A.; Liu, Q.; Wu, P. Effect of pre-deformation on the activation stress of {10–12} twinning in Mg-3Al-1Zn alloy. *Mater. Sci. Eng. A* **2021**, *800*, 140384. [[CrossRef](#)]
14. Xin, Y.C.; Wang, M.Y.; Zeng, Z.; Nie, M.G.; Liu, Q. Strengthening and toughening of magnesium alloy by {10–12} extension twins. *Scr. Mater.* **2012**, *66*, 25–28. [[CrossRef](#)]
15. Song, B.; Xin, R.L.; Sun, L.Y.; Chen, G.; Liu, Q. Enhancing the strength of rolled ZK60 alloys via the combined use of twinning deformation and aging treatment. *Mater. Sci. Eng. A Struct. Mater. Prop. Microstruct. Process.* **2013**, *582*, 68–75. [[CrossRef](#)]
16. Song, B.; Guo, N.; Liu, T.T.; Yang, Q.S. Improvement of formability and mechanical properties of magnesium alloys via pre-twinning: A review. *Mater. Des.* **2014**, *62*, 352–360. [[CrossRef](#)]
17. Xin, Y.C.; Wang, M.Y.; Zeng, Z.; Huang, G.J.; Liu, Q. Tailoring the texture of magnesium alloy by twinning deformation to improve the rolling capability. *Scr. Mater.* **2011**, *64*, 986–989. [[CrossRef](#)]
18. Barnett, M.R. Influence of deformation conditions and texture on the high temperature flow stress of magnesium AZ31. *J. Light Met.* **2001**, *1*, 167–177. [[CrossRef](#)]
19. Knezevic, M.; Levinson, A.; Harris, R.; Mishra, R.K.; Doherty, R.D.; Kalidindi, S.R. Deformation twinning in AZ31: Influence on strain hardening and texture evolution. *Acta Mater.* **2010**, *58*, 6230–6242. [[CrossRef](#)]
20. Wang, B.S.; Xin, R.L.; Huang, G.J.; Liu, Q. Strain rate and texture effects on microstructural characteristics of Mg-3Al-1Zn alloy during compression. *Scr. Mater.* **2012**, *66*, 239–242. [[CrossRef](#)]
21. Chen, P.; Wang, F.X.; Li, B. Dislocation absorption and transmutation at {10–12} twin boundaries in deformation of magnesium. *Acta Mater.* **2019**, *164*, 440–453. [[CrossRef](#)]
22. Chen, P.; Li, B.; Culbertson, D.; Jiang, Y. Negligible effect of twin-slip interaction on hardening in deformation of a Mg-3Al-1Zn alloy. *Mater. Sci. Eng. A* **2018**, *729*, 285–293. [[CrossRef](#)]
23. Hong, S.G.; Park, S.H.; Lee, C.S. Role of {10–12} twinning characteristics in the deformation behavior of a polycrystalline magnesium alloy. *Acta Mater.* **2010**, *58*, 5873–5885. [[CrossRef](#)]
24. Sun, Q.; Xia, T.; Tan, L.; Tu, J.; Zhang, M.; Zhu, M.; Zhang, X. Influence of {10–12} twin characteristics on detwinning in Mg-3Al-1Zn alloy. *Mater. Sci. Eng. A Struct. Mater. Prop. Microstruct. Process.* **2018**, *735*, 243–249. [[CrossRef](#)]
25. Park, S.H.; Lee, J.H.; Huh, Y.-H.; Hong, S.-G. Enhancing the effect of texture control using {10–12} twins by retarding detwinning activity in rolled Mg-3Al-1Zn alloy. *Scr. Mater.* **2013**, *69*, 797–800. [[CrossRef](#)]
26. Li, Y.P.; Cui, Y.J.; Bian, H.K.; Sun, S.H.; Tang, N.; Chen, Y.; Liu, B.; Koizumi, Y.; Chiba, A. Detwinning in Mg alloy with a high density of twin boundaries. *Sci. Technol. Adv. Mater.* **2014**, *15*, 8. [[CrossRef](#)] [[PubMed](#)]
27. Jiang, L.; Jonas, J.J.; Luo, A.A.; Sachdev, A.K.; Godet, S. Influence of {10–12} extension twinning on the flow behavior of AZ31 Mg alloy. *Mater. Sci. Eng. A* **2007**, *445–446*, 302–309. [[CrossRef](#)]
28. Yu, H.; Xin, Y.; Wang, M.; Liu, Q. Hall-Petch relationship in Mg alloys: A review. *J. Mater. Sci. Technol.* **2018**, *34*, 248–256. [[CrossRef](#)]
29. Yu, H.H.; Xin, Y.C.; Chapuis, A.; Huang, X.X.; Xin, R.L.; Liu, Q. The different effects of twin boundary and grain boundary on reducing tension-compression yield asymmetry of Mg alloys. *Sci. Rep.* **2016**, *6*, 8. [[CrossRef](#)]
30. Wang, L.H.; Teng, J.; Wu, Y.; Sha, X.C.; Xiang, S.S.; Mao, S.C.; Yu, G.H.; Zhang, Z.; Zou, J.; Han, X.D. In situ atomic scale mechanisms of strain-induced twin boundary shear to high angle grain boundary in nanocrystalline Pt. *Ultramicroscopy* **2018**, *195*, 69–73. [[CrossRef](#)]
31. Sun, Q.; Zhang, X.Y.; Ren, Y.; Tu, J.; Liu, Q. Interfacial structure of {10–12} twin tip in deformed magnesium alloy. *Scr. Mater.* **2014**, *90–91*, 41–44. [[CrossRef](#)]